Aeolian Research 46 (2020) 100615

Contents lists available at ScienceDirect

Aeolian Research

journal homepage: www.elsevier.com/locate/aeolia

Magnetic susceptibility parameters as proxies for desert sediment provenance

Lars Petter Hällberg[a,*], Thomas Stevens[b], Bjarne Almqvist[b], Ian Snowball[b], Steffen Wiers[b], Chiara Költringer[b], Huayu Lu[c], Hanzhi Zhang[c], Zeng Lin[d]

[a] Department of Geological Sciences, Stockholm University, Svante Arrhenius väg 8C, 10691 Stockholm, Sweden
[b] Department of Earth Sciences, Uppsala University, Villavägen 16, 75236 Uppsala, Sweden
[c] School of Geography and Ocean Science, Nanjing University, 210023 Nanjing, China
[d] School of Resources and Environmental Engineering, Ludong University, 264025 Yantai, China

ARTICLE INFO

Keywords:
Magnetic susceptibility
Frequency dependence
Agico Kappabridge
Acreo DynoMag
Mu Us Desert
Provenance

ABSTRACT

Magnetic susceptibility in sediments has been thoroughly studied as a paleoenvironmental proxy over the last decades. However, it is unknown to what extent magnetic susceptibility variation is also a diagnostic of different sediment sources. Here we investigate if multiple magnetic susceptibility-based parameters can effectively be used as sediment source indicators. New magnetic property data from the Mu Us and Tengger Deserts in China are compared to previously known sediment provenance based on other well-established proxies. To assess the magnetic properties of these deserts, magnetic susceptibility and its out-of-phase component, its dependence on frequency, temperature and low-field amplitude are analyzed. Our results indicate similar sources for the western Mu Us Desert and the Tengger Desert and a distinct source for the eastern Mu Us, in-line with previously hypothesized provenance patterns. However, magnetic properties within the Tengger Desert sediments are homogenous, which may suggest a uniform provenance for the entire Tengger Desert, that the sediments are greatly reworked, or similar magnetic properties in potential multiple source regions. Magnetite is the major magnetic mineral in the study area and the dominant causes for divergence in magnetic properties are the magnetic mineral concentration and domain state. The results here, in particular from the Mu Us, suggest considerable promise for using magnetic susceptibility parameters in desert sediment provenance research.

1. Introduction

Magnetic susceptibility (κ) of sediments has been intensely studied during the last decades, mainly as a proxy for paleoenvironment and past climate variations (e.g., Heller and Evens, 1995, Baosheng et al., 2000, Porter, 2001, Dong et al., 2015) or sediment relative age dating through stratigraphic correlation, particularly in loess (e.g., Ding et al., 2001, Hao and Guo, 2007, Marković et al., 2015, Zhao et al., 2016). κ variations through loess sequences are considered to be caused by environmental factors such as soil formation under warm and humid conditions. However, κ is chiefly affected by the concentration and types of iron oxides, which in part may also be driven by changes in source sediments (Sun and Liu, 2000, Maher, 2011, Zan et al., 2019). Despite this, identifying provenance is still a relatively underexplored aspect of the technique (Wang et al., 2017a). Here, the potential of magnetic susceptibility to be utilized in the field of sediment provenance is investigated in detail. This is achieved by examining a range of magnetic susceptibility-based parameters using an Agico MFK1-FA Kappabridge and an Acreo DynoMag system. A good test of whether provenance can be assessed via magnetic susceptibility parameters is found in the Mu Us Desert, which is an intensely studied region in terms of provenance and displays a well-constrained shift in sediment provenance across its area. The Mu Us sandy land (area with currently stabilized dunes - hereafter referred to as desert for simplicity), as well as the nearby Tengger Desert, have also been hypothesized to be potential dust sources for the Chinese Loess Plateau (CLP) (Sun et al., 2020, Stevens et al., 2013, Sun et al., 2008), the world's most extensive and well-studied aeolian dust deposit and paleoenvironmental archive

Abbreviations: χ_{lf}, magnetic susceptibility measured at 976 Hz; χ_{hf}, magnetic susceptibility measured at 15615 Hz; χ_{fd}, frequency dependence of magnetic susceptibility; χ_{fn}, normalised frequency dependence of magnetic susceptibility; χ_{on}, normalised out-of-phase magnetic susceptibility parameter; δ, phase parameter; T_c, Curie temperature

* Corresponding author.
E-mail address: petter.hallberg@geo.su.se (L.P. Hällberg).

https://doi.org/10.1016/j.aeolia.2020.100615
Received 13 January 2020; Received in revised form 15 May 2020; Accepted 18 May 2020

(Guo et al., 2002, Lu et al., 2010, Nie et al., 2010, Nie et al., 2016). The CLP and aeolian dust transportation in China has received much attention (e.g., Qian et al., 2018, Licht et al., 2016, Nie et al., 2015, Pullen et al., 2011, Sun, 2002) as airborne dust activity has an extensive impact on the Earth system. It affects desert spreading rates, global nutrient cycling, the Earth's radiation balance, and can act as cloud condensation nuclei (see e.g., Wang et al., 2017b, Loveley et al., 2017, Kok et al., 2017, Vinoj et al., 2014). Understanding aeolian sediment provenance is a major part of determining the role of dust in climate variations (Nie et al., 2018, Jickells et al., 2005, Rea et al., 1988), and analysis of potential dust sources such as deserts for provenance signatures is an essential part of this.

The provenance of the Mu Us Desert (Fig. 1) has previously been studied through a number of techniques, including single grain U-Pb zircon dating, heavy mineral analysis, zircon morphology, fission track dating/zircon double dating, and framework petrography (e.g., Stevens et al., 2010, Stevens et al., 2013, Nie et al., 2015, Bird et al., 2015, Zhang et al., 2013, 2016, 2018, Wang et al., 2019a, Sun et al., 2020), bulk geochemical indices (Sun, 2002, Rao et al., 2008) and electron spin resonance and quartz crystallinity (Sun et al., 2008, 2013). Detailed results from single grain provenance analysis show that the provenance of the Mu Us Desert sands can be roughly divided into a western (or south-western) part and an eastern (or north-eastern) part, both with different sediment origins (Stevens et al., 2013, Bird et al., 2015, Nie et al., 2015, Zhang et al., 2016, Wang et al., 2019a). It should be noted though that the exact position of the hypothesized line between 'east' and 'west' is rather variable and some samples close to each other but either side of this division display starkly different provenance signals (Stevens et al., 2013, Zhang et al., 2016, Wang et al., 2019a). The eastern part has derived a large part of its sediment from the underlying bedrock in Mu Us and the Ordos plateau just north of Mu Us, while the western part has received its sediment mainly from the Yellow River, originating from the north-eastern Tibetan Plateau (Stevens et al., 2013, Nie et al., 2015, Sun et al., 2020). Both parts of the desert also receive windblown material from the Gobi Desert in the north and northwest (Zhang et al., 2013, 2016). The adjacent Tengger Desert (Fig. 1) has not been as intensely studied, but likely has a different provenance history (e.g., Chen et al., 2007, Sun et al., 2008, Sun et al., 2013, Zhang et al., 2013, 2016, Fan et al., 2019, Sun et al., 2020). Although heavy mineral analyses are not conclusive, zircon U-Pb dating of Tengger Desert sediment suggests a Yellow River and Tibetan Plateau source for the southern parts of the desert, similar to western Mu Us provenance, while the northern part is dominated by Gobi Desert sediment input (Zhang et al., 2016). Sun et al. (2020) compiled previously published provenance data from electron spin resonance, quartz δ18O, Sr-Nd isotopes and U-Pb and reported overlap or a small difference between Tengger and Mu Us in each parameter and suggests that the main source for Mu Us and Tengger sediment is the northern Tibetan Plateau, with a likely additional input from Ordos plateau in the northern Mu Us.

Magnetic susceptibility of rocks and sediments varies with mineral composition and magnetic domain states. Different rocks and sediments therefore have different magnetic susceptibility signals, and in many environmental magnetic studies, the influence of lithology on magnetic properties has been noted (e.g., Sun and Liu, 2000, Ding et al., 2001, Nie et al., 2007, Wang et al., 2017a). Magnetic susceptibility has also been shown to function as a sediment tracer during aeolian erosion events (Ravi et al., 2019). Maher et al. (2009) found differences in magnetic susceptibility and geochemical data across the last glacial loess of the Chinese Loess Plateau and between different Gobi Desert sediments. Based on this observation they hypothesized that magnetic susceptibility may be used to determine provenance of sediments in this region. Maher (2011) reports that aeolian sediment deposits across the world have susceptibility signals that are characteristic for their location, source rocks and environments. These characteristics may also be valid at the intraregional scale and, therefore, used as a dust provenance tool. Liu et al. (2015) measured a range of magnetic properties in desert surface sediments in China and Mongolia and found distinct signals for different deserts, further supporting this hypothesis. The advantages of magnetic susceptibility as a provenance tool, if this technique proves successful, is that available instruments are highly sensitive (Hrouda and Pokorny, 2011) and measurements are cheap, rapid, non-destructive and easily conducted with minimal sample preparation, enabling large datasets to be collected, which is essential in provenance research.

Here we test the hypothesis that magnetic susceptibility-based

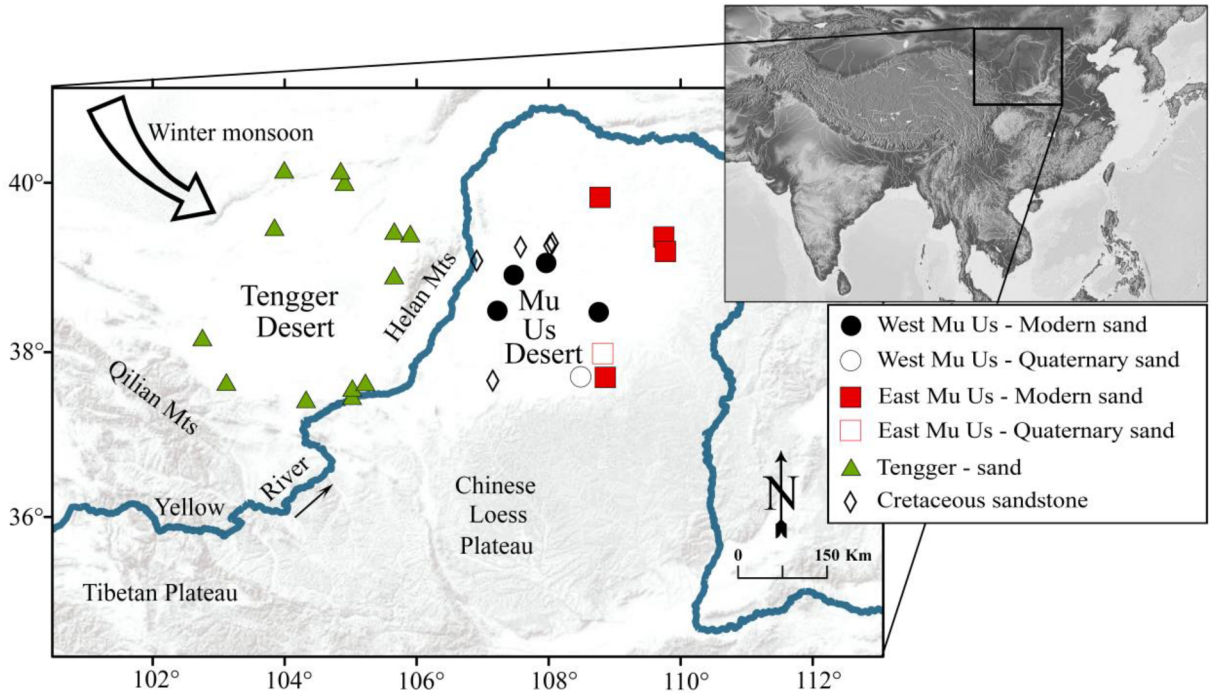

Fig. 1. Map of the northern China study area and location of samples in the Mu Us and Tengger Deserts. Base map data obtained from OpenStreetMap.

parameters give the same provenance results as other well-established provenance techniques. This is done by analysing the magnetic properties of surface sediments collected from a region with clear and well-constrained provenance differences. We further apply the method by examining a region where the provenance is less well known, in an attempt to make predictions according to the magnetic susceptibility data for that region. The well-studied Mu Us and the adjacent Tengger Deserts in China (Fig. 1) are ideal candidates for this test.

2. Background of magnetic susceptibility analyses

Here, multiple magnetic properties derived primarily from Agico Kappabridge MFK1-FA (Pokorný et al., 2011) susceptibility equipment are evaluated and compared to provenance studies to infer if provenance is a cause for variation in magnetic susceptibility in the study area. The specific measurement details for the different parameters used in this study are described in the Methods section, but here an outline of the principles behind the use of the different parameters is given. κ is measured at low field amplitude (typically around 200 A/m) and reflects how readily a material is magnetised when subjected to an applied magnetic field. Mass specific magnetic susceptibility (χ) is then calculated as $\chi = \kappa * V/m$ where V is sample volume and m is the sample mass (Snowball, 1999). χ at low frequency (χ_{lf}) along with its frequency dependence (χ_{fd}): the percentage loss of χ between low and high frequency measurements, are often used as paleoclimatic and paleoenvironmental proxies in loess (Maher, 2011). χ_{fd} enhancement is indicative of the presence of ultrafine (< ~25 nm: Maher, 1988) and highly magnetisable superparamagnetic (SP) particles that are formed in situ, mainly during soil formation (Liu et al, 2005a). In this monsoon marginal Chinese setting, this is associated with warm and humid conditions under a strong summer monsoon favouring biological activity, while low values of χ_{fd} are associated with cold and arid conditions and strong winter monsoon where soil formation is limited and sediment input is high (Porter, 2001). Formation of highly magnetic SP particles can also drive enhancement of χ_{lf}, which is why both χ_{lf} and χ_{fd} have been used independently as proxies for climate driven pedogenesis (Balsam et al., 2011, Liu et al., 2017). As the Tengger and Mu Us Deserts are semi-arid to arid regions with limited biological activity, the rates of weathering and pedogenesis in the sediments are generally low. This implies that weathering and pedogenesis are not the main controls of χ_{lf} and χ_{fd} of surface sediments in this region, which may rather be signatures inherited from the source lithology.

In addition to these standard measures, the χ of sediments can be measured while varying other key measurement conditions. Measuring the variation of χ over a large range of temperatures, typically from −192 to 700 °C, yields information on the mineral composition of the magnetic mineral fraction (Liu et al., 2005b). As a ferromagnetic mineral is heated above its Curie temperature (T_c) χ sharply decreases as the mineral transitions into a paramagnetic state and this transition temperature is specific for each mineral (Dunlop and Özdemir, 1997, Hrouda, 2003). For antiferromagnetic minerals, this transition is referred to as Néel temperature. Other mineral specific temperature dependent characteristics include the Verwey transition of magnetite (change in crystal structure resulting in peak χ at approximately −150 °C) and the Morin transition of hematite at approximately −25 °C, below which the weak ferromagnetic properties of the mineral are lost and χ decreases (Evans and Heller, 2003). χ can further be measured while varying the amplitude of the applied field. The field amplitude dependence of the resultant χ reflects the magnetic mineral composition of the bulk sample (Hrouda et al., 2006, Jackson et al., 1998) and in the case of magnetite has a different sign depending on if the magnetite fraction is dominated by single-domain (SD) or multi-domain (MD) grains (Hrouda et al., 2006). Furthermore, to examine how the magnetic susceptibility varies as a function of frequency, we examine χ over a large (100 kHz) frequency range at high resolution on selected samples using an Acreo DynoMag system.

3. Study area and sediment provenance

The study area consists of two sandy deserts bordering the Chinese Loess Plateau in northern China: the Mu Us and the Tengger Deserts (Fig. 1). Mean annual air temperatures are approximately 7 °C (http://data.cma.cn/en). There is a south-easterly gradient of increasing precipitation in the region with ~100 mm/year in north-western Tengger (http://data.cma.cn/en) and 380 mm/year in south-eastern Mu Us (Hu et al., 2012, Liu et al., 2017). Sand dunes cover large parts of both areas but are mostly stabilized in the more humid Mu Us, leading to a classification as 'sandy land' in Chinese nomenclature. The Mu Us is underlain by Cretaceous sandstone (Liu and Yang, 2000, Zhang et al., 2013, Kapp et al., 2015) of aeolian origin, which in many areas crops out through the overlying Quaternary fluvial and aeolian sediments, especially in the north-western Mu Us (Li et al., 1999). This sandstone is highly weathered as indicated by analysis of its heavy mineral assemblages (Stevens et al., 2013, Bird et al., 2015). The surface and Quaternary sediments in the Mu Us Desert exhibit a shift in provenance from its western to eastern parts. Western (or south-western) Mu Us zircons exhibit two prominent age peaks at ~250 Ma and ~450 Ma (Stevens et al., 2013, Zhang et al., 2016), concurrent with zircon ages from the northern Tibetan Plateau (Pullen et al., 2011) and the upper Yellow River (Stevens et al., 2013, Nie et al., 2015, Licht et al., 2016). The eastern (or north-eastern) Mu Us and the underlying Cretaceous bedrock exhibit a single dominant age peak at ~ 250 Ma and secondary age peaks at 1500 and 2750 Ma, indicating that the Cretaceous bedrock is the source for the eastern Mu Us sand (Stevens et al., 2013, Zhang et al., 2013, 2016, Bird et al., 2015, Licht et al., 2016). Gobi Desert sediment input from the north may also be substantial for most parts of the Mu Us Desert (Zhang et al., 2013, 2016). The provenance differences observed in zircon age distributions between the eastern (or north-eastern) and western (or south-western) Mu Us Desert are also reflected in the heavy mineral composition (Stevens et al., 2013, Wang et al., 2019a). The eastern Mu Us surface sands and underlying Cretaceous sandstones have a more mature heavy mineral composition dominated by the stable mineral garnet, while the western Mu Us is dominated by less stable amphibole and epidote (Stevens et al., 2013, Bird et al., 2015).

Less is known of the sediment provenance in the adjacent Tengger Desert but it is likely, at least in part, different from the Mu Us, as indicated by electron spin resonance and quartz crystallinity (Sun et al., 2008, Sun et al., 2013) isotopic data (Chen et al., 2007) and zircon typology (Zhang et al., 2013). The Tengger Desert formed around 0.9 Ma when the large lake that previously covered the area dried out (Fan et al., 2018). Zircon U-Pb dating indicates that the southern part of the desert contains the double age distribution peaks between ~250 Ma and ~450 Ma, which would indicate a Tibetan Plateau/Yellow River source, (Stevens et al., 2013, Zhang et al., 2016) similar to the western Mu Us, consistent with heavy mineral data (Stevens et al., 2013, Nie and Peng, 2014). Southern Tengger also exhibits obvious age peaks between 1300 and 2800 Ma, which is more similar to eastern Mu Us and indicates input from additional sources (Stevens et al., 2013, Zhang et al., 2016, Fan et al., 2019). These sources have been hypothesized to be a mix from the underlying North China Craton, consisting of Archean and Proterozoic crystalline rocks (Zhao et al., 2005, Zhang et al., 2013), the Gobi Altai Mountains and the north-eastern Tibetan Plateau (Zhang et al., 2013, 2016). The northern part of the Tengger Desert exhibits the

single dominating age peak at ~280 Ma (Stevens et al., 2010, Zhang et al., 2016), but this is only partly supported by the zircon ages reported from the north-western Tengger by other studies. Licht et al. (2016) report prominent peaks at ~270 Ma and ~450 Ma. Down-core U-Pb dating in north-western Tengger reveals the double age peak at ~250 and ~450 Ma for the most recent samples indicating a Tibetan Plateau/Yellow River source also in the north (Fan et al., 2019). Fan et al. (2019) also show that the provenance has shifted over time in Tengger, with higher input from the Gobi Altai Mountains to the north before 0.62 Ma. Wang et al., (2019b) compared goethite, hematite and element geochemistry between north-eastern Tibetan Plateau (Qilian Mountains) derived river sediments and the north Tengger Desert. They found similar signatures, suggesting a genetic link, in particular for the silty component. Based on a dimension reducing visualization technique applied to multi-proxy datasets, Bird et al. (2015) showed that east central Tengger sediments are most similar to the eastern Mu Us and the Cretaceous sandstones which underlie the Mu Us. However, this was based only on a single sample from eastern Tengger Desert and is not supported by heavy mineral assemblage data for the same sample which shows similarity to western Mu Us (Stevens et al., 2013, Nie and Peng, 2014).

4. Material

A total of 32 samples are analysed in this study (Table 1), collected over a large geographical spread in the Tengger and Mu Us Deserts (Fig. 1) in 2008, 2009, 2011 and 2012 at elevations ranging from 1107 to 1730 m a.s.l. Of these, 19 samples were collected from modern surface aeolian sand while five samples of poorly lithified Cretaceous sandstones from the Mu Us Desert represent the underlying bedrock. Three sediment samples from the Mu Us Desert are of Quaternary age and collected from two different locations in the Sjara-Osso-Gol formation along the Honglui River. Sample MW5 is aeolian sand while ME5 and ME6 are from the same section, with the former an aeolian sand near the top of the section and the latter fluvially deposited sand from the base of the section. Four samples from the Tengger Desert are taken from a section on an alluvial fan below the Helan mountains (TG11, TG12, TG13 and TG14, ordered from section base to modern surface). TG11 consists of pink sand, possibly of Pliocene age, while the overlying sediments are interpreted to be of Quaternary to modern age. TG15 is from a dried out braided river channel in northern Tengger Desert. TG16 is taken from a fluvial section on Shiyang River which drains the Qilian Mountains. The Mu Us samples are divided at 108.77 °E into an eastern and western group based on suggestion from Stevens et al. (2013) and the data observed in this study.

5. Methods

Bulk samples were first oven-dried at 45 °C and then approximately 10 g of each was placed in 7 cm^3 plastic containers. Magnetic susceptibility and phase components were measured at the Department of Earth Sciences, Uppsala University, using an Agico Kappabridge MFK1-FA at 200 A/m field amplitude and frequencies of 976 Hz and 15615 Hz. Each sample was measured five times and parameters were averaged (arithmetic mean). To validate the results, all samples were remeasured for χ and χ_{fd} twice, including a run on another identical instrument at the Department of Geological Sciences, Stockholm University. The original patterns shown in the data remained the same, despite variability in the absolute values of χ_{fd}. To further test the repeatability of these results, a subset of samples was analyzed with an Acreo DynoMag at frequencies ranging from 5 to 100,000 Hz. The following calculations were done using data from the Agico Kappabridge MFK1-FA: χ_{fd} was calculated as $\chi_{fd}\ (\%) = 100\ (\chi_{lf}-\chi_{hf})/\chi_{lf}$ where χ_{lf} and χ_{hf} are the magnetic susceptibilities measured at low and high frequency. χ_{fn} represents the normalized version of the frequency dependence and allows better comparison of data obtained using different instruments (Hrouda, 2011). χ_{fn} was calculated as $\chi_{fn}\ (\%) = \chi_{fd}/(\ln F_{hf} - \ln F_{lf})$ where F_{lf} and F_{hf} are the low and high operating frequencies used by the magnetic susceptibility meter, respectively. χ_{on} measures the out-of-phase contribution to magnetic susceptibility (Hrouda et al., 2013) and was calculated as $\chi_{on}\ (\%) = (200/\pi) * \tan \delta_{lf}$, where δ_{lf} is the phase angle measured at low frequency. Applied field amplitude dependence (here after referred to as field dependence) of χ was measured by incrementally increasing the applied field amplitude from 75 to 700 A/m at the 976 Hz operating frequency and calculated as $Field\ dependence\ (\%) = 100*(\chi_{700A/m}-\chi_{75A/m})/\chi_{75A/m}$. The temperature dependence of χ was measured on bulk samples at 200 A/m field amplitude and 976 Hz operating frequency. Low temperature measurements were conducted using a cryostat cooled by liquid nitrogen to −196 °C and subsequently heated to 0 °C. High temperature measurements were carried out in an argon atmosphere to prevent oxidation using a MFK1-FA equipped with a CS4 furnace attachment. Samples were heated from room temperature up to 700 °C at an approximate rate of 11.8 °C/min, held for 5 min at 700 °C, and subsequently cooled to 40 °C while χ was continuously measured. The values were corrected by subtracting the χ of the empty cryostat

Table 1
Sample information.

Sample group	Number of samples, approx. age & origin	Sample names
Mu Us – West	4 Modern – aeolian	MW1, MW2, MW3, MW4
	1 Quaternary – aeolian	MW5
Mu Us – East	4 Modern – aeolian	ME1, ME2, ME3, ME4
	1 Quaternary – aeolian	ME5
	1 Quaternary – fluvial	ME6
Mu Us bedrock	5 Cretaceous – poorly lithified aeolian sandstone	CS1, CS2, CS3, CS4, CS5
Tengger	11 Modern – aeolian	TG1, TG2, …, TG10, TG14
	1 Pliocene – fluvial	TG11
	4 Quaternary – fluvial	TG12, TG13, TG15, TG16

and furnace. Determination of Curie/Néel temperatures were undertaken in Agico Cureval8 by analysing thermomagnetic curves as χ and $1/\chi$ against temperature.

On commonly used magnetic susceptibility bridges such as the Bartington MS2 and Agico Kappabridge, κ is measured in an alternating field (Hrouda et al., 2015). Magnetic susceptibility is normally determined in-phase with the applied field at maximum amplitude, calculated as $\kappa = M/H_{max}$ where κ is magnetic susceptibility, M is magnetisation and H_{max} is the applied field at the maximum amplitude. However, most materials exhibit a phase lag that results in a measurable magnetic susceptibility when the applied field is zero (Hrouda et al., 2013). This is referred to as out-of-phase magnetic susceptibility (Jackson, 2003–2004, Hrouda et al., 2013, 2017, 2018, 2014, Nie et al., 2008) and is calculated as $\kappa" = M"/H_{max}$ where $\kappa"$ is out-of-phase susceptibility, $M"$ is the magnetisation when the applied field is zero and H_{max} is the applied field at its maximum amplitude. The phase lag can also be expressed as an angle $\delta = arctan(\kappa"/\kappa)$ and is referred to as phase (Hrouda et al., 2013). Out-of-phase susceptibility may arise for several reasons: 1) viscous relaxation due to presence of magnetic particles near the superparamagnetic – stable single domain (SP - SD) grain size boundary; 2) electrical eddy currents (induced by the AC field in conductive materials) and; 3) weak field hysteresis (nonlinear and irreversible dependence of M on H). If the phase lag is due to viscous relaxation, the out-of-phase susceptibility should correlate well with normalized frequency dependence of in-phase magnetic susceptibility (for more information and reasoning, see Hrouda et al., 2013). Hrouda (2011) introduced the parameters for the normalized frequency dependence (χ_{fn}) and out-of-phase susceptibility (χ_{on}) in order to investigate the relationship between in- and out-of-phase susceptibility.

6. Results

Temperature dependence of χ was measured on all Mu Us samples and on six samples from the Tengger Desert. The most distinct change in the thermomagnetic curves for all samples is the drop in χ around 580 °C, the known Curie temperature (T_C) of pure magnetite (Table 2). Thermomagnetic curves for representative, magnetite dominated samples are presented in Fig. 2a and c, and for samples that are different from pure magnetite in Fig. 2b and d. There are weak traces of secondary Néel/Curie points at higher temperatures for some samples, however this is without a clear geographical pattern. At low temperature, all samples except CS2 have peaks in χ at −150 °C. CS2 has a clear peak in χ at −173 °C (Fig. 2b) and a small secondary peak at that temperature is also observed for ME1. An increase in χ around −25 °C is observed in TG8 (Fig. 2b) and modestly in TG3. The samples from Tengger display a sharper decrease in susceptibility around 580 °C and very little decrease beyond that temperature compared to the other regions.

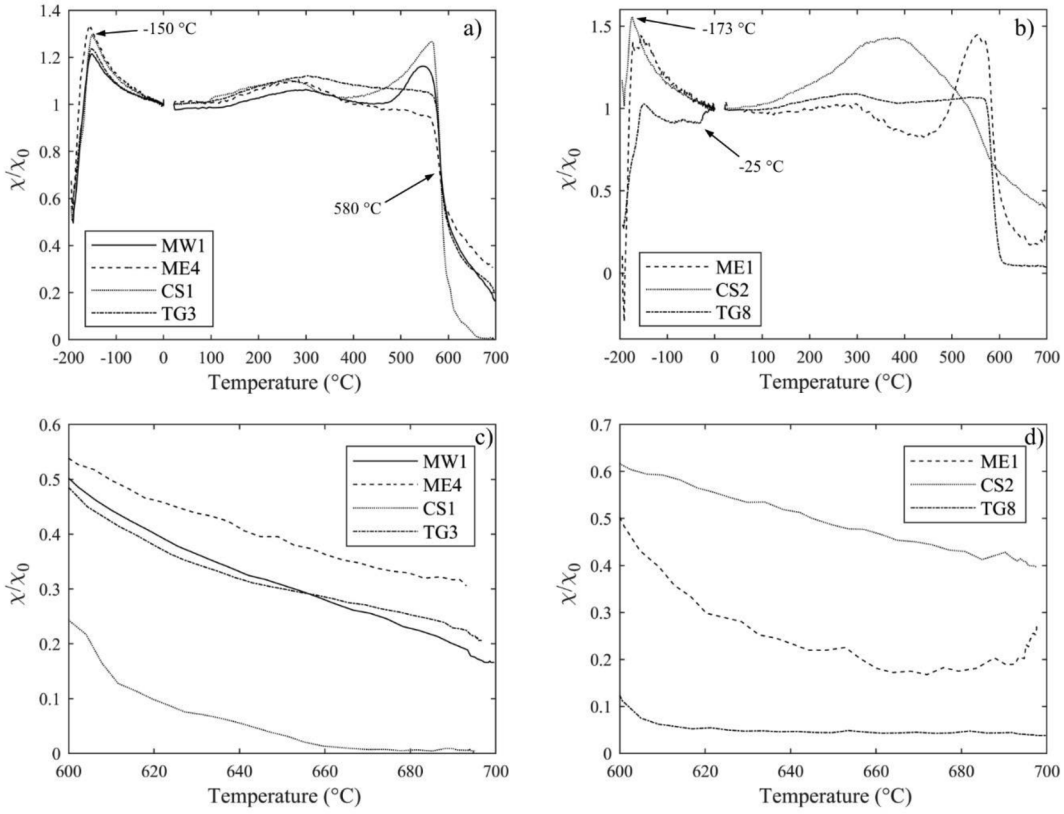

Fig. 2. Temperature dependence of magnetic susceptibility for a) magnetite dominated samples and b) samples that are different from pure magnetite. c) and d) show the temperature dependence between 600 and 700 °C, i.e. above the Curie temperature for magnetite. χ is normalised against the magnetic susceptibility at room temperature χ_0.

Field dependence of χ is very low for all samples, below 1% change in χ between 75 and 700 A/m applied field. 30 out of the 32 samples show statistically significant linear trends at 95% confidence level and at the 99% confidence level, 26 of the samples show statistically significant linear trends. Samples from western Mu Us and Tengger have positive field dependence while Cretaceous sandstone and eastern Mu

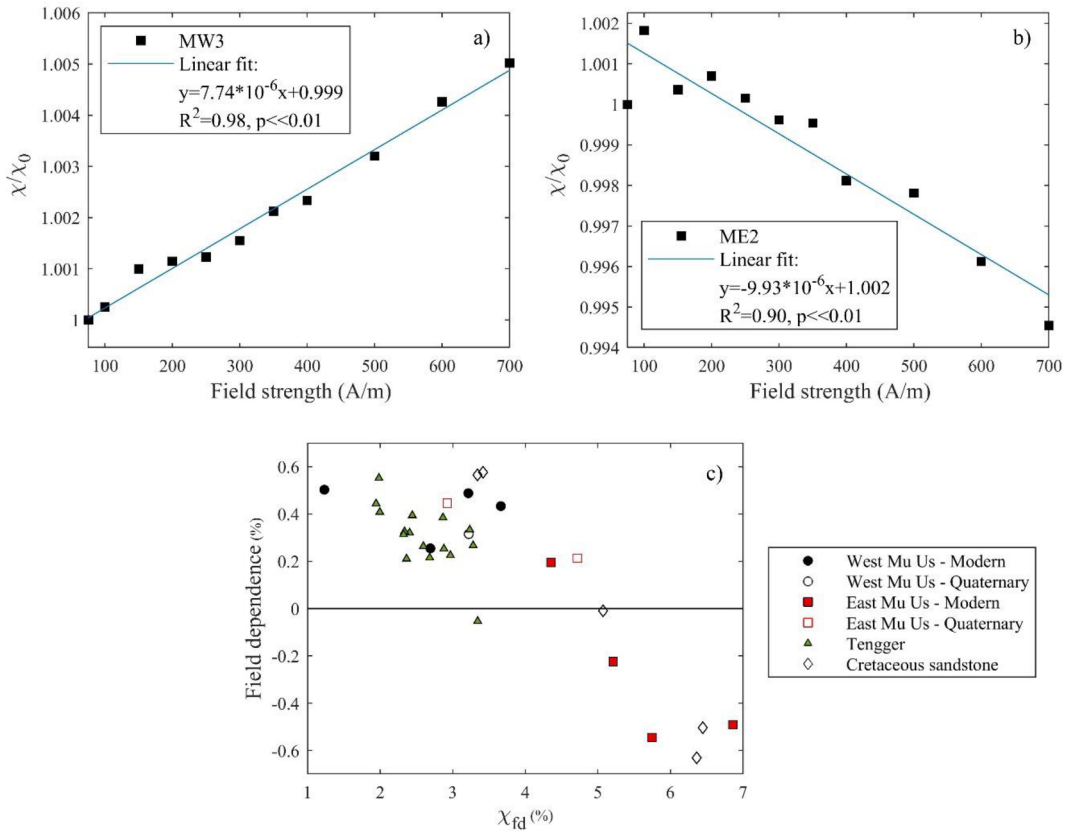

Fig. 3. Field dependence plots for a) sample MW3 and b) sample ME2. Black squares represent individual measurements and the blue line represents the best fit linear model. c) Field dependence plotted against frequency dependence χ_{fd}. (For interpretation of the references to colour in this figure legend, the reader is referred to the web version of this article.)

Table 2
Results and location for each sample.

Sample name	χ_{lf} 10^{-8} m^3kg^{-1}	χ_{fd} %	χ_{fn} %	χ_{on} %	Field dep. %	T_c °C	δ_{lf} °	Long. °N	Lat. °E
MW1	28.6	2.69	0.97	1.18	0.25	578	1.06	38.49228	107.2270
MW2	18.0	3.21	1.16	1.21	0.49	566	1.09	38.91685	107.4753
MW3	46.6	1.23	0.44	1.04	0.50	580	0.93	39.05965	107.9663
MW4	28.3	3.66	1.32	1.10	0.43	570	0.99	38.47682	108.7627
MW5	27.0	3.22	1.16	1.28	0.32	577	1.15	37.70575	108.4881
ME1	9.9	6.86	2.47	2.38	−0.49	578	2.14	39.83280	108.7817
ME2	5.6	5.74	2.07	2.57	−0.55	561	2.31	39.36832	109.7474
ME3	17.6	4.35	1.57	1.57	0.20	578	1.42	39.19853	109.7732
ME4	15.6	5.21	1.88	1.63	−0.32	580	1.47	37.70097	108.8626
ME5	19.9	2.92	1.05	1.14	0.45	570	1.03	37.98703	108.8221
ME6	5.5	4.72	1.70	1.95	0.21	571	1.76	37.98703	108.8221
CS1	43.1	3.34	1.20	0.84	0.56	580	0.76	39.29428	108.0593
CS2	16.8	6.45	2.32	2.52	−0.5	559	2.26	39.08742	106.9122
CS3	8.5	5.07	1.83	2.21	−0.01	579	1.99	39.24682	107.5770
CS4	9.3	3.42	1.23	1.61	0.58	578	1.45	39.26528	108.0208
CS5	1.8	6.36	2.29	3.72	−0.63	569	3.34	37.65887	107.1567
TG1	69.0	1.98	0.72	1.15	0.55	579	1.03	39.40712	105.9062
TG2	26.0	2.88	1.04	1.08	0.25		0.97	39.43610	105.6639
TG3	44.1	2.00	0.72	0.88	0.41	583	0.79	40.14143	104.8519
TG4	32.3	2.34	0.84	0.89	0.33		0.80	40.15075	103.9968
TG5	33.5	2.32	0.84	0.87	0.31	590	0.78	39.48103	103.8488
TG6	24.7	2.36	0.85	1.01	0.11		0.91	37.64180	103.1212
TG7	20.4	2.68	0.97	1.02	0.22		0.92	37.43390	104.3271
TG8	44.3	2.60	0.94	0.76	0.26	577	0.69	37.47183	105.0243
TG9	15.6	3.34	1.21	1.11	−0.05		1.00	37.57045	105.0288
TG10	31.3	2.87	1.03	0.90	0.38		0.81	37.63860	105.2264
TG11	10.4	2.44	0.88	0.67	0.39	578	0.60	38.91262	105.6615
TG12	38.1	1.94	0.70	0.78	0.44	576	0.71	38.91262	105.6615
TG13	31.7	2.41	0.87	0.96	0.32		0.87	38.91262	105.6615
TG14	25.2	3.28	1.18	1.12	0.27		1.01	38.91262	105.6615
TG15	30.5	3.23	1.17	0.97	0.33		0.87	40.00760	104.9122
TG16	28.8	2.97	1.07	1.01	0.23		0.91	38.17607	102.7579

Us samples show both positive and negative field dependences (Fig. 3 and Table 2). There is a negative correlation between field dependence and frequency dependence (Fig. 3c).

Within the Mu Us Desert there is a clear pattern in the magnetic susceptibility and frequency dependence data (Fig. 4). In the samples from the western part of the desert, χ_{lf} is elevated and χ_{fd} is low ($29.7 \pm 10.4*10^{-8}$ m^3kg^{-1} and $2.8 \pm 0.9\%$ respectively). The eastern part of the Mu Us Desert displays low χ_{lf} and high χ_{fd} ($12.35 \pm 6.2*10^{-8}$ m^3kg^{-1} and $5.0 \pm 1.3\%$ respectively), which is similar to results from the Cretaceous sandstone samples ($15.9 \pm 16.1*10^{-8}$ m^3kg^{-1} and $4.9 \pm 1.5\%$ respectively). This pattern is also supported by measurements undertaken on the Acreo DynoMag (Fig. 5). We note that the eastern Mu Us samples also show considerably more variable χ with changing frequency than the western Mu Us samples. Tengger Desert samples all display elevated χ_{lf} values and low χ_{fd} ($31.6 \pm 13.47*10^{-8}$ m^3kg^{-1} and $2.6 \pm 0.45\%$ respectively). There is a consistent negative correlation between magnetic susceptibility and frequency dependence in all sample groups.

The out-of-phase component of magnetic susceptibility χ_{on} follows the same pattern between regions as in-phase magnetic susceptibility,

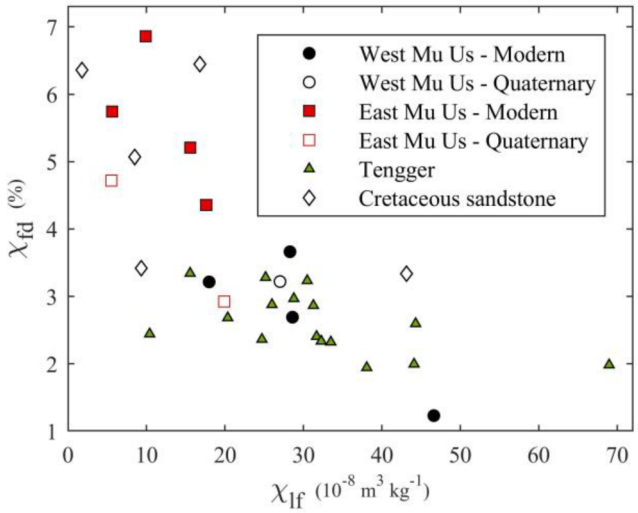

Fig. 4. Frequency dependence χ_{fd} versus magnetic susceptibility χ_{lf}.

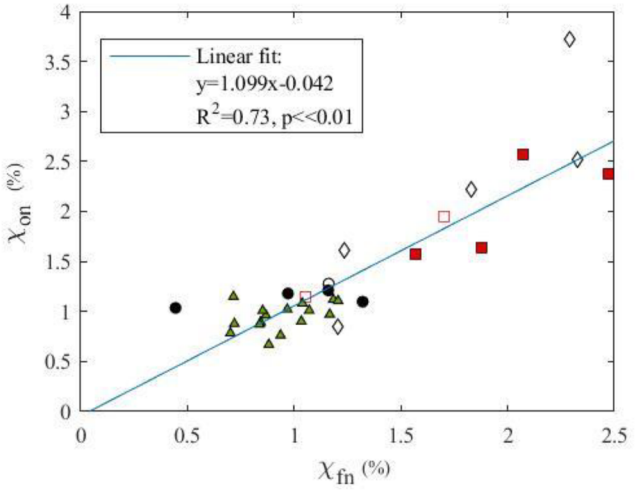

Fig. 6. The out-of-phase parameter χ_{on} versus normalized frequency dependence parameter χ_{fn}. The blue line represents the best fit. Symbols as in Fig. 3. (For interpretation of the references to colour in this figure legend, the reader is referred to the web version of this article.)

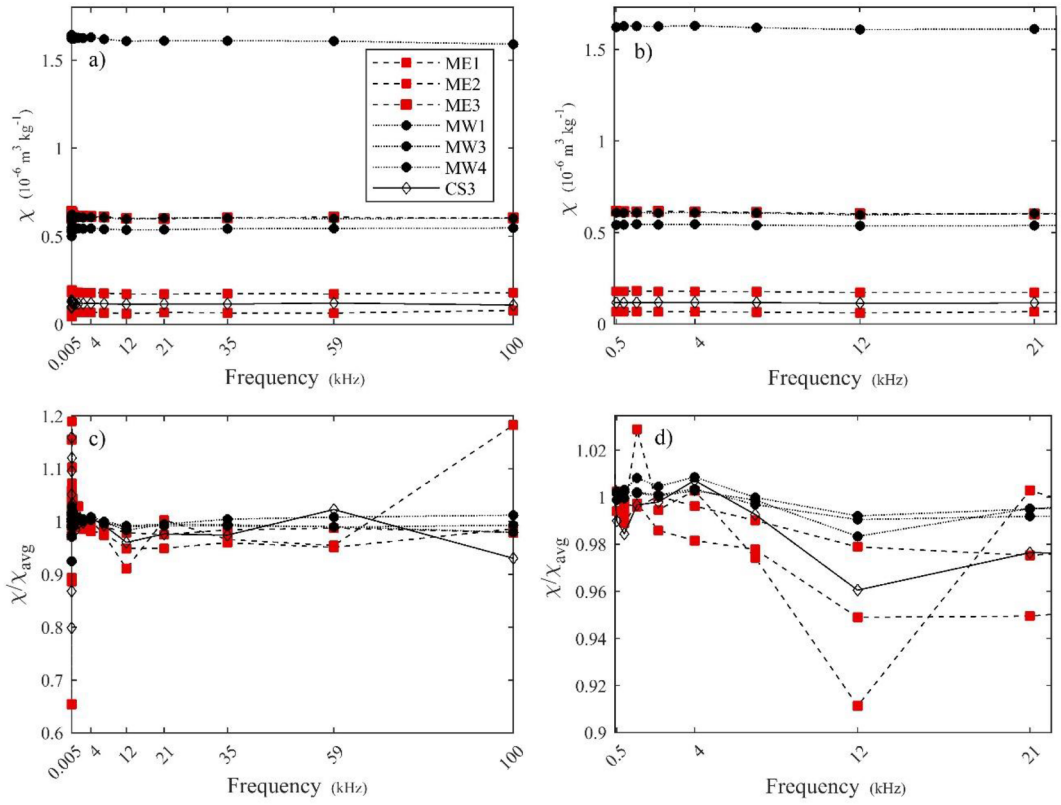

Fig. 5. Mass corrected magnetic susceptibility measured in multiple steps over a 100 kHz frequency range. a) and b) χ versus frequency, and c) and d) χ normalised to average χ versus frequency. b) and d) are zoomed in to the 0.5–21 kHz frequency to highlight the range of common magnetic susceptibility meters.

χ_{fd}. The lowest values are observed in the western Mu Us and Tengger samples, while the eastern Mu Us and Cretaceous samples have higher values. There is a high correlation between χ_{on} and the normalized frequency dependence parameter χ_{fn} (Fig. 6), the linear fit model has a slope of 1.099 and intercept of −0.042, R^2-value is 0.73 with a p-value < 0.1.

7. Reproducibility of magnetic susceptibility measurements

Repeat measurements of χ_{lf} and χ_{fd} on the Agico Kappabridge show that the general patterns between the regions are reproducible between measurement runs (Fig. 7a and b). However, the absolute values, in particular for χ_{fd} vary between measurement runs (Fig. 7e and Table 3). Since the changes in χ between the low and high frequency measurements (Fig. 7c and d) are generally just a few percent, any small uncertainty or variability in the instrument or laboratory environment will have a considerable impact on the calculated value of χ_{fd} (Fig. 7e and Table 3). The variation between runs causing this deviation in χ_{fd} is similar in both χ_{lf} and χ_{hf}. The average absolute value differences between the original measurements (conducted in Uppsala 2017) and the second measurements (conducted in Uppsala 2018) are $1.05*10^{-8}$ m^3kg^{-1} for χ_{lf}, $0.85*10^{-8}$ m^3kg^{-1} for χ_{hf} and 4.27% for χ_{fd}. The average difference between the original measurements and the measurements at the identical instrument at Stockholm University in 2019 are $1.09*10^{-8}$ m^3kg^{-1} for χ_{lf} and $1.25*10^{-8}$ m^3kg^{-1} for χ_{hf} and 1.39% for χ_{fd}.

To validate our results further, an independent repeatability test was conducted on a subset of samples using an Acreo DynoMag system, which measures χ at frequencies from 5 to 100,000 Hz, a much larger range at higher resolution than the Kappabridge. The DynoMag measurements reproduce the pattern recorded by the Agico Kappabridge, with western Mu Us displaying high χ (Fig. 5a and b) and very small

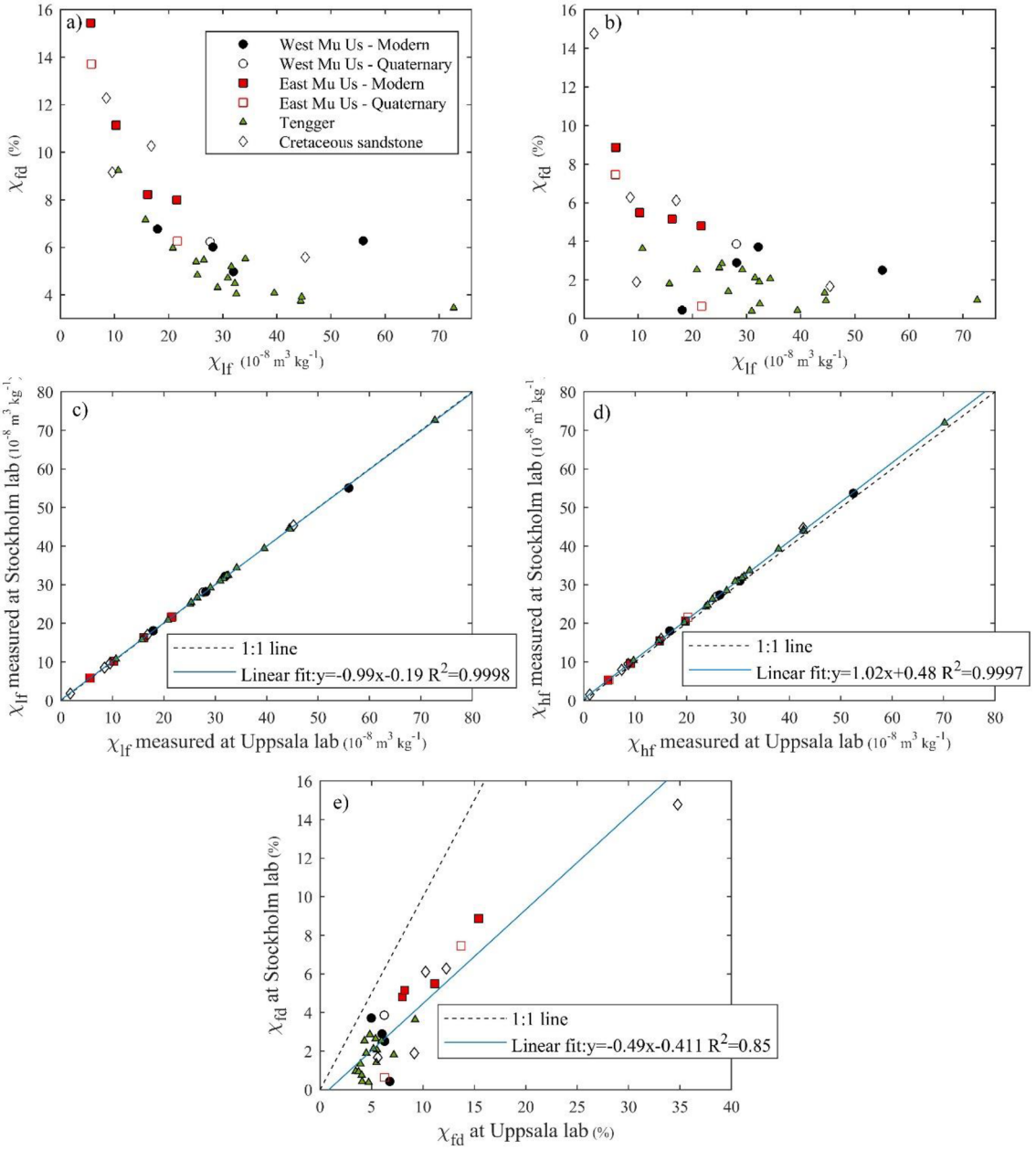

Fig. 7. Magnetic susceptibility and its frequency dependence remeasured a) in 2018 on the same Agico Kappabridge MFK1-FA instrument in Uppsala and b) on an identical MFK1-FA at Stockholm University in 2019. Note that one outlier (sample CS5) at 35% χ_{fd} is not shown in a). c) and d) show the data from respective remeasurement run against each other for χ_{lf}, χ_{hf} and e) χ_{fd} calculated using the data displayed in c) and d).

Table 3
χ_{lf}, χ_{hf} and χ_{fd} from original measurements on an Agico Kappabridge MFK1-FA in Uppsala lab in 2017, remeasurements on the same instrument in 2018, and on an identical instrument at Stockholm University in 2019.

	Uppsala 2017			Uppsala 2018			Stockholm 2019		
Sample name	χ_{lf} 10^{-8} m^3kg^{-1}	χ_{hf} 10^{-8} m^3kg^{-1}	χ_{fd} %	χ_{lf} 10^{-8} m^3kg^{-1}	χ_{hf} 10^{-8} m^3kg^{-1}	χ_{fd} %	χ_{lf} 10^{-8} m^3kg^{-1}	χ_{hf} 10^{-8} m^3kg^{-1}	χ_{fd} %
MW1	28.61	27.84	2.69	28.16	26.47	6.02	28.17	27.35	2.89
MW2	17.98	17.40	3.21	17.94	16.73	6.77	18.10	18.02	0.43
MW3	46.63	46.05	1.23	55.97	52.45	6.28	55.08	53.69	2.51
MW4	28.29	27.25	3.66	31.96	30.37	4.97	32.19	30.99	3.71
MW5	27.02	26.15	3.22	27.68	25.96	6.23	28.11	27.03	3.86
ME1	9.90	9.22	6.86	10.25	9.11	11.14	10.27	9.71	5.49
ME2	5.59	5.27	5.74	5.57	4.71	15.43	5.83	5.31	8.86
ME3	17.59	16.83	4.35	21.48	19.76	8.00	21.61	20.57	4.81
ME4	15.59	14.78	5.21	16.08	14.76	8.22	16.26	15.43	5.15
ME5	19.90	19.32	2.92	21.63	20.28	6.27	21.69	21.55	0.64
ME6	5.53	5.27	4.72	5.71	4.93	13.71	5.79	5.36	7.46
CS1	43.13	41.69	3.34	45.24	42.71	5.59	45.40	44.64	1.66
CS2	16.82	15.73	6.45	16.80	15.07	10.26	17.00	15.96	6.11
CS3	8.48	8.05	5.07	8.46	7.42	12.28	8.50	7.97	6.28
CS4	9.33	9.01	3.42	9.56	8.68	9.16	9.67	9.49	1.89
CS5	1.77	1.66	6.36	1.82	1.18	34.76	1.80	1.53	14.78
TG1	68.98	67.61	1.98	72.71	70.19	3.46	72.63	71.94	0.96
TG2	25.99	25.24	2.88	26.49	25.04	5.47	26.62	26.25	1.40
TG3	44.11	43.23	2.00	44.40	42.74	3.74	44.68	44.27	0.93
TG4	32.27	31.52	2.34	32.52	31.21	4.04	32.45	32.20	0.76
TG5	33.50	32.72	2.32	34.17	32.28	5.53	34.37	33.66	2.07
TG6	24.71	24.13	2.36	25.09	23.74	5.40	24.96	24.30	2.64
TG7	20.35	19.81	2.68	20.81	19.56	5.97	20.80	20.27	2.53
TG8	44.31	43.16	2.60	44.60	42.85	3.92	44.42	43.83	1.33
TG9	15.55	15.03	3.34	15.72	14.59	7.16	15.75	15.46	1.81
TG10	31.27	30.38	2.87	31.60	29.96	5.18	31.58	30.91	2.12
TG11	10.40	10.14	2.44	10.69	9.70	9.23	10.76	10.37	3.63
TG12	38.07	37.33	1.94	39.52	37.91	4.08	39.42	39.26	0.42
TG13	31.68	30.92	2.41	32.22	30.77	4.49	32.37	31.75	1.90
TG14	25.18	24.35	3.28	25.31	24.08	4.84	25.43	24.71	2.85
TG15	30.49	29.50	3.23	30.94	29.48	4.72	30.99	30.87	0.38
TG16	28.78	27.92	2.97	29.06	27.81	4.31	29.23	28.49	2.54

dependence on frequency (Fig. 5c and d), while the eastern Mu Us and the Cretaceous sandstone samples have lower χ, which decreases significantly at higher frequency. The reproducibility of the χ patterns in the DynoMag data appears to be very good, as shown in three repeat runs on the same sample (Fig. 8), indicating that the differences observed between samples are not a function of instrumental uncertainty.

Considering that the observed patterns are repeated in three independent measurement runs on two Agico Kappabridge MFK1-FA instruments and also on a DynoMag system we are confident that the results are robust and derive from a real property of the material rather than measurement error. However, the poor reproducibility in absolute values of χ_{fd} is interpreted as an intrinsic issue arising from minute

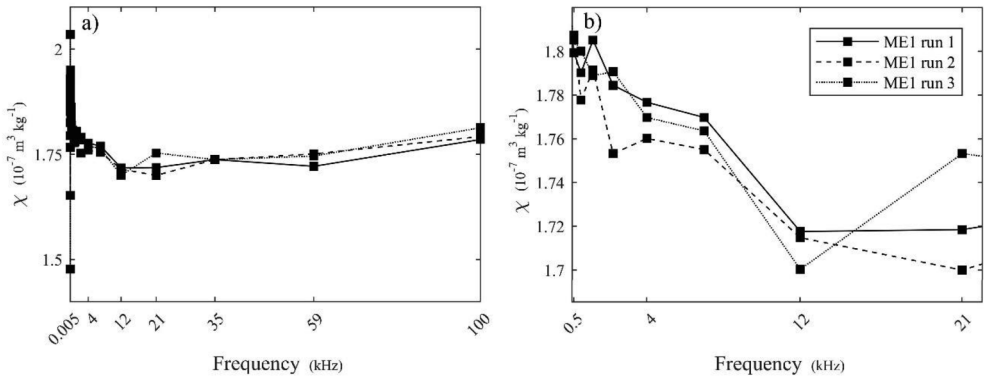

Fig. 8. Sample ME1 measured under three repeat measurement sequences comprising a) 20 measurements between 5 and 100,000 Hz on the Acreo DynoMag and b) zoomed in to the 0.5–21 kHz frequency to highlight the range of common magnetic susceptibility meters.

uncertainties in magnetic susceptibility meters and how the χ_{fd} parameter is defined. Comparing χ_{fd} values across studies where absolute susceptibility and χ_{fd} is relatively low must thus be undertaken with great caution, even with the generally more sensitive Agico Kappabridge MFK1-FA.

8. Discussion

Out-of-phase and in-phase magnetic susceptibility as well as their dependence on field amplitude and frequency display regional differences within the study area. There is a clear difference between the western and eastern parts of the Mu Us Desert. The Cretaceous sandstone samples are more similar to the eastern Mu Us samples while the Tengger samples are more similar to the western parts of the Mu Us. This pattern is in agreement with suggested sediment provenance differences based on previous research and indicates that the magnetic properties examined here reflect the provenance of the sediments (Bird et al., 2015, Nie et al., 2015, Stevens et al., 2013, Zhang et al., 2013, 2016, Wang et al., 2019a, Sun et al., 2020). Here, the relevance of each parameter is discussed.

The Curie temperature is around 580 °C for all samples, indicating magnetite presence and that changes in the concentration of magnetite will likely determine variations in low field magnetic susceptibility in the entire study area (Evans and Heller, 2003). Minor secondary drops in susceptibility around the Curie/Néel temperatures for maghemite (645 °C but can range from 590 to 675 °C and maghemite may be transformed into hematite from around 300 °C) and hematite (675 °C) were also observed in some samples, which is interpreted to indicate presence of those minerals (Evans and Heller, 2003, Gehring et al., 2009). Maghemite and hematite presence is however not specific to any specific region in the study area and we do not base any conclusions on their presence in single samples. The Tengger samples display lower contents of hematite and maghemite based on the sharper decrease in χ at the T_C of magnetite near 580 °C. In all samples except CS2, peaks in χ are observed at −150 °C. These are interpreted as indicative of Verwey transitions; the transition of magnetite crystal structure from monoclinic to cubic inverse spinel (Dunlop and Özdemir 1997, Carter-Stiglitz et al., 2006). In CS2, χ peaks at −173 °C, where a possible origin for the signal can be a depressed Verwey transition temperature due to the presence of non-stochiometric magnetite (Aragón et al., 1985). χ increases at approximately −25 °C in samples TG8 (Fig. 2) and TG3. This is indicative of the Morin transition, which suggests the presence of hematite (Özdemir et al., 2008), but this is only very weakly supported by a decrease in χ around the Néel temperature of hematite for TG8, and not at all for TG3.

The almost field amplitude independent χ of all studied samples is typical for pure magnetite (Hrouda et al., 2006, Jackson et al., 1998) providing independent verification that magnetite is the dominant magnetic mineral in all samples. Minor (but statistically significant) dependencies on the applied field amplitude are however observed for most samples (Fig. 3). The statistical analysis shows that the linear trends on 30 out of 32 samples are statistically significant at 95% confidence interval and that 26 sample trends are statistically significant at 99% confidence interval. This implies that the measurements are precise and the field dependence observed, despite being low, reflects a real physical property of the sediments. Western Mu Us and Tengger samples display a positive dependence on field, while the eastern Mu Us and the Cretaceous sandstone samples have a mix of both positive and negative dependencies. Weakly positive field dependence is indicative of MD magnetite and weakly negative field dependence is indicative of SD magnetite (Hrouda et al., 2006) which suggests that the susceptibility of western Mu Us and Tengger are dominated by larger (MD) magnetite grains and that the eastern Mu Us and Cretaceous sandstones consists of a both SD and MD magnetite grains.

Frequency dependence of χ shows a clear difference between the regions. The values are higher in the eastern Mu Us and the Cretaceous sandstone samples and lower in the western Mu Us and Tengger samples (Fig. 4). Enhanced χ_{fd} suggests elevated content of magnetic particles at the SD and SP boundary (Maher, 2007, Liu et al., 2004). Overall, out-of-phase magnetic susceptibility as well as field- and frequency-dependent magnetic susceptibilities all point to regional differences in magnetic mineral particle size; higher contents of fine to ultrafine SD and SP magnetite in the eastern Mu Us sands and the Cretaceous sandstones, whereas western Mu Us and Tengger samples contain more relatively coarse MD magnetite. In Chinese aeolian loess deposits, χ_{fd} usually correlates with χ_{lf}, due to weathering/pedogenesis and subsequent production of highly magnetizable ultrafine SP grains, which is the dominant source for enhancement of both signals (Maher, 2011). Here, by contrast the χ_{lf} is decreased for the samples that contain greater proportions of SP particles – the opposite to what we would expect if pedogenic processes were responsible for SP magnetite formation and enhanced χ_{fd} and χ_{lf}. If the properties observed in the χ_{lf} and χ_{fd} data in the eastern Mu Us are not the result of provenance differences/changes, two processes are required to simultaneously act upon the modern/Quaternary sediments to explain the observed values: formation of 1) SP particles via pedogenesis, and 2) alteration of strongly magnetic iron oxides into less magnetic versions. Those two co-occurring processes would probably require acidic or anoxic waterlogged conditions (Maher, 1998), which are unlikely in coarse grained desert surface sediments. Alternatively, the low χ_{lf} could be explained by formation of hematite, which has much lower χ_{lf} than magnetite, but this is not supported by our thermomagnetic data as the χ_{lf} signal in these samples are dominated by magnetite. This suggests that the magnetic mineral grain size differences in the samples have not developed as a consequence of pedogenesis/weathering but are instead a signature of the source rocks themselves, including the Cretaceous sandstone which is the hypothesized source for the eastern Mu Us sediments. We therefore conclude that the magnetic susceptibility signal is dominated by SD and MD particles that cause increases in bulk susceptibility but decreases in frequency dependence, rather than pedogenic products (i.e., SP particles) which would cause increases in both parameters. A possible mechanism for the low concentration of SP particles in the western Mu Us could be the relative enrichment of coarser, stable particles such as quartz and removal or destruction of SP particles during fluvial transport of source materials by the Yellow River. Further supporting our interpretation, Liu et al. (2017) found that precipitation (which can drive pedogenesis) only has a statistically significant impact on χ_{fd} in the south-western corner of the Mu Us (with highest precipitation) but not further north. Their data also show a negative correlation between χ_{lf} and precipitation – the opposite to what would be expected if precipitation was driving production of highly magnetisable SP grains. While it cannot be ruled out that the precipitation gradient in the region has some influence on the magnetic properties observed here, it is certainly not the main driver of χ_{fd}. Liu et al. (2017) proposes that lithological differences may be a dominant driver of χ_{fd} in the Mu Us Desert except in the south-western part, in agreement with our results and interpretation. No sample in this study is from the south-western part of Mu Us where the correlation with precipitation was found in Liu et al.'s (2017) study.

There is a high correlation between the out-of-phase χ_{on} and normalized frequency dependence χ_{fn} parameters across the study area. The slope of the straight fit line between χ_{fn} and χ_{on} parameters is approximately 1 and the intercept is near $y = 0$ (Fig. 6), while the field dependence is low. This indicates that the cause for phase enhancement is viscous relaxation of ultrafine magnetic particles at the SP-SD boundary present in the sample (Hrouda et al., 2013, Jackson, 2003–2004). In this case the phase lag parameter yields effectively the same information as χ_{fd}, implying that the use of out-of-phase susceptibility may be a complement to frequency dependence in examining the presence of ultrafine particles in sediments.

Five of the Mu Us samples presented here have been used in previous provenance research. Stevens et al. (2013) analysed MW1, MW3,

MW4 and ME6 (sample codes in that paper MD-9, MD-2, MD-3 and MD-5 respectively) amongst other samples for heavy mineral assemblage and U-Pb zircon ages and found that the Mu Us samples could be divided into an eastern and a western group, based on this data. MW1/MD-9 and MW3/MD-3 were in the western group and MW4/MD-2 and ME6/MD-5 in the eastern group. Our χ data concur with this in three out of the four samples. MW4/MD-2, a sample from central Mu Us very near the east to west boundary, does not match that pattern in terms of phase, χ_{lf} and field dependence. The χ_{fd} is slightly enhanced compared to the other western Mu Us samples and overlaps with both regions. The disparity of the magnetic data and the provenance indicators could be an effect of local differences in weathering intensities between sites. However, magnetic minerals are not considered in the zircon U-Pb nor heavy mineral analysis, which also could lead to some variations in results between methods due to different source controls on magnetic mineralogy versus heavy mineral/zircon composition. Considering that the sample is located near the boundary between the eastern and western Mu Us, sediments carrying 'western Mu Us' magnetic properties may be mixed with an 'eastern Mu Us' heavy mineral composition and zircon age distribution. Bird et al. (2015) analysed heavy mineral composition and U-Pb ages of CS5 (sample code in their paper CH11-MU-01) and their results concur with Stevens et al.'s (2013) that the Cretaceous sandstone bedrock is highly depleted in certain heavy minerals due to weathering and has a similar composition to the eastern Mu Us sediments. It therefore seems likely that the low χ_{lf} and high χ_{fd} seen in the eastern Mu Us is imported from the Cretaceous sandstone bedrock. This implies that the magnetic differences in the Mu Us indeed reflects a provenance signal of the local sedimentary Cretaceous sandstone bedrock versus the Yellow River sourced sediments in western Mu Us. This analysis also underscores the importance of multiproxy provenance analyses approaches (Nie et al., 2012), where different techniques target different mineral components of the sediments.

9. Implications for provenance

For the Mu Us Desert the results are encouraging in terms of the ability of the techniques to differentiate between sediment sources. This is seen in the χ data from the disparity of the western and eastern parts of the desert as well as the similarity of the eastern sand samples and the underlying Cretaceous sandstone. In terms of sediment provenance relationship between the Mu Us and Tengger Deserts, the magnetic properties of western Mu Us are very similar to the adjacent Tengger Desert. This is in-line with other studies in that the source of parts of both the Tengger and western Mu Us is likely to be dominated by the Yellow River/northern Tibetan Plateau sediments (Stevens et al., 2013, Nie et al., 2015, Zhang et al., 2016). In contrast to the patterns in the Mu Us data, there are no systematic differences within the Tengger Desert in any of the measured parameters. Based on U-Pb dating, Zhang (2016) suggests a Yellow River/north eastern Tibetan Plateau source for the sediments in the south-western and south-eastern edges of Tengger, and a Gobi source dominating for in the rest of the Tengger Desert. However, the provenance of Tengger remains uncertain and complex as indicated by evidence that does not support Gobi Desert input into the northern parts of Tengger (Fan et al., 2019) and a north-eastern Tibetan Plateau source for northern Tengger sediments (Wang et al., 2019b). The magnetic data presented here reveals no pattern in the Tengger Desert. χ has a relatively large range but lacks a spatial pattern, while out-of-phase susceptibility, frequency-, field- and temperature-dependence are homogenous for the entire desert. This could be indicative of either a uniform provenance for the entire desert, that the sediments are greatly reworked and homogenized, or that its source regions would have uniform magnetic properties (even if being different in for example, zircon ages). This deserves further study and the exact sediment provenance characteristics of the Tengger remain enigmatic.

10. Conclusions

This study aims to evaluate if a combination of magnetic susceptibility-based parameters can be used to infer sediment provenance in a semi-arid to arid region. The Mu Us Desert comprises sediments of different origin between its eastern and western parts, as demonstrated in multiple previous studies. Here, this source difference is also reflected in multiple magnetic susceptibility parameters. As such magnetic susceptibility and its dependence on frequency, low-field amplitude and temperature can be a useful tool in desert sediment provenance research, especially with the analysis of multiple parameters.

- The eastern part of the Mu Us Desert displays low magnetic susceptibility, but elevated contents of SD and SP particles seen in a range of magnetic susceptibility-based parameters. This is interpreted as a signal arising from its hypothesized main source – the underlying Cretaceous sandstone bedrock.
- In the western Mu Us Desert and the Tengger Desert, the higher magnetic susceptibility is due to higher concentrations of relatively coarse single and multi-domain magnetite. The similarity in magnetic properties between these areas suggests a similar sediment origin.
- Magnetic mineral concentration and magnetic domain states in these regions appears to be governed by primary source lithology, rather than secondary processes, and are interpreted as the main causes for magnetic susceptibility differences in the Mu Us Desert.
- The Tengger Desert's magnetic properties are homogenous within the desert and do not show a clear pattern, indicating either a uniform provenance for the entire Tengger Desert, that the sediments are well-mixed, or that similar magnetic properties in multiple source region lithologies render the technique unsuitable as a provenance indicator for internal differences within the Tengger Desert.
- Out-of-phase magnetic susceptibility correlates with normalized frequency dependence of magnetic susceptibility, supporting the suggestions of Hrouda et al. (2013) that out-of-phase magnetic susceptibility can be used as an independent proxy for SP particle concentration.
- The magnetic susceptibility variability with applied field frequency clearly contrasts between the eastern and western Mu Us Desert samples analysed here. The origin for these different patterns in the high resolution 100 kHz frequency measurement range remains to be explored.
- Suitable regions for using magnetic susceptibility parameters as provenance indicators are likely to be arid environments, without extensive weathering and pedogenesis active in the surface sediments, as these processes are known to influence and modify the magnetic properties.

CRediT authorship contribution statement

Lars Petter Hällberg: Investigation, Formal analysis, Writing - original draft. **Thomas Stevens:** Writing - review & editing, Supervision, Investigation, Methodology. **Bjarne Almqvist:** Writing - review & editing. **Ian Snowball:** Writing - review & editing. **Steffen Wiers:** Writing - review & editing. **Chiara Költringer:** Writing - review & editing. **Huayu Lu:** Writing - review & editing, Funding acquisition. **Hanzhi Zhang:** Writing - review & editing. **Zeng Lin:** Writing - review & editing.

Declaration of Competing Interest

The authors declare that they have no known competing financial interests or personal relationships that could have appeared to influence the work reported in this paper.

Acknowledgements

The field campaigns were partly supported by a grant from the National Natural Science foundation of China awarded to Lu (no. 41920104005) and by a Natural Environment Research Council (NERC) grant (UK) to TS (NE/I008837/1). We want to thank Matt O'Regan and Gabriel West at the Department of Geological Sciences, Stockholm University for assistance and access to their Agico Kappabridge. We are indebted to three anonymous reviewers whose comments significantly improved this manuscript.

References

Aragón, R., Shepherd, J.P., Koenitzer, J.W., Buttery, D.J., Rasmussen, R.J., Honig, J.M., 1985. Influence of nonstochiometry on the Verwey transition in Fe3(1-δ) O4. J. Appl. Phys. 57 (3221), 10 1063/1.335156.

Balsam, W.L., Ellwood, B.B., Ji, J., Williams, E.R., Long, X., Hassani, A., 2011. Magnetic susceptibility as a proxy for rainfall: Worldwide data from tropical and temperate climate. Quat. Sci. Rev. 30, 2732–2744. https://doi.org/10.1016/j.quascirev.2011.06.002.

Baosheng, L., Zhang, D.D., Heling, J., Zheng, W., Mancun, Y., Wu, S., Yizhi, Z., Donghuai, S., 2000. Paleomonsoon activities of Mu Us Desert, China since 150 ka B.P. – A study of stratigraphic sequences of the Milanggouwan Section, Salawusa River area. Paleogeogr., Paleoclimatol., Paleoecol. 162, 1–16. https://doi.org/10.1016/S0031-0182(00)00101-2.

Bird, A., Stevens, T., Rittner, M., Vermeesch, P., Carter, A., Ando, S., Garzanti, E., Lu, H., Nie, J., Zeng, L., Zhang., Xu, Z., 2015. Quaternary dust source variation across the Chinese Loess Plateau Paleogeography. Paleoclimatol., Paleoevol. 435, 254–264. https://doi.org/10.1016/j.palaeo.2015.06.024.

Carter-Stiglitz, B., Moskowitz, B., Solheid, P., Berquo, T.S., Jackson, M., Kosterov, A., 2006. Low-temperature magnetic behaviour of multidomain titanomagnetites: TM0, TM16, and TM35. J. Geophys. Res. 111, B12S05. https://doi.org/10.1029/2006JB004561.

Chen, J., Li, G., Yang, J., Rao, W., Lu, H., Balsam, W., Sun, Y., Ji, J., 2007. Nd and Sr isotopic characteristics of Chinese Deserts: Implications for the provenances of Asian dust. Geochim. Cosmochim. Acta 71, 3904–3914. https://doi.org/10.1016/j.gca.2007.04.033.

Ding, Z.L., Yang, S.L., Sun, J.M., Liu, T.S., 2001. Iron geochemistry of loess and red clay deposits in the Chinese Loess Plateau and implications for long-term Asian monsoon evolution in the last 7.0 Ma. Earth Planet. Sci. Lett. 185, 99–109. https://doi.org/10.1016/S0012-821X(00)00366-6.

Dong, Y., Wu, N., Li, F., Huang, L., Wen, W., 2015. Time-transgressive nature of the magnetic susceptibility record across the chinese loess plateau at the pleistocene/holocene transition. PLoS One 10 (7), e0133541. https://doi.org/10.1371/journal.pone.0133541.

Dunlop, D., Özdemir, Ö., 1997. Rock Magnetism Fundamentals and Frontiers. Cambridge University Press. https://doi.org/10.1017/CBO9780511612794.

Evans, M.E., Heller, F., 2003. Environmental Magnetism. Academic Press, Principles and Applications of Enviromagnetics.

Fan, Y., Mou, X., Wang, Y., Liu, C., Zhao, H., Wang, F., Li, Z., Mao, X., Liu, W., Ma, J., Liu, C., Zhang, F., Zhang, 2018. Quaternary paleoenvironmental evolution of the Tengger Desert and its implications for the provenance of the loess of the Chinese Loess Plateau. Quat. Sci. Rev. 197, 21–34. https://doi.org/10.1016/j.quascirev.2018.08.002.

Fan, Y., Li, Z., Wang, F., Ma, J., Mou, X., Li, X., Zhang, Q., Zhao, H., Chen, F., 2019. Provenance variations of the Tengger Desert since 2.35 Ma and its linkage with the Northern Tibetan Plateau: Evidence from U-Pb age spectra of detrital zircons. Quat. Sci. Rev. 223. https://doi.org/10.1016/j.quascirev.2019.105916.

Gehring, A.U., Fischer, H., Louvel, M., Kunze, K., Weidler, P.G., 2009. High temperature stability of natural maghemite: A magnetic and spectroscopic study. Geophys. J. I. 179, 1361–1371. https://doi.org/10.1111/j.1365-246X.2009.04348.x.

Guo, Z.T., Ruddiman, W.F., Hao, Q.Z., Wu, H.B., Qlao, Y.S., Zhu, R.X., Peng, S.Z., Wei, J.J., Yuan, B.Y., Liu, T.S., 2002. Onset of Asian Desertification by 22 Myr ago inferred from loess deposits in China. Nature 416, 159–163.

Hao, Q., Guo, Z., 2007. Magnetostratigraphy of an early-middle Miocene loess-soil sequence in the western Loess Plateau of China. Geophys. Res. Lett. 34, L18305. https://doi.org/10.1029/2007GL031162.

Heller, F., Evans, E.M., 1995. Loess magnetism. Rev. Geophys. 33, 211–240. https://doi.org/10.1029/95RG00579.

Hrouda, F., 2003. Indices for numerical characterization of the alteration processes of magnetic minerals taking place during the investigation of temperature variatio of magnetic susceptibility. Stud. Geophys. Geod. 47, 847–861.

Hrouda, F., Chlupacova, M., Mrazova, S., 2006. Low-field variation of magnetic susceptibility as a tool for magnetic mineralogy of rocks. Phys. Earth Planet. Inter. 154, 323–336. https://doi.org/10.1016/j.pepi.2005.09.013.

Hrouda, F., Pokorny, J., 2011. Extremely high demands for measurement accuracy in precise determination of frequency-dependent magnetic susceptibility of rocks and soils. Stud. Geophys. Geod. 55, 667–681. https://doi.org/10.1007/s11200-010-0079-6.

Hrouda, F., 2011. Models of frequency-dependent susceptibility of rocks and soils revisited and broadened. Geophys. J. Int. 187, 1259–1269. https://doi.org/10.1111/j.1365-246X.2011.05227.x.

Hrouda, F., Pokorny, J., Jazek, J., Chadima, M., 2013. Out-of-phase magnetic susceptibility of rocks and soils: A rapid tool for magnetic granulometry. Geophys. J. Int. 194, 170–181. https://doi.org/10.1093/gji/ggt097.

Hrouda, F., Pokorny, J., Chadima, M., 2015. Limits of out-of-phase susceptibility in magnetic granulometry of rocks and soils. Stud. Geophys. Geod. 59, 294–308. https://doi.org/10.1007/s11200-014-0948-5.

Hrouda, F., Chadima, M., Jezek, J., Pokorny, J., 2017. Anisotropy of out-of-phase magnetic susceptibility of rocks as a tool for direct determination of magnetic subfabrics of some minerals: an introductory study. Geophys. J. Int. 208, 385–402. https://doi.org/10.1093/gji/ggw399.

Hrouda, F., Chadima, M., Jezek, J., Kadlec, J., 2018. Anisotropies of in-phase, out-of-phase, and frequency-dependent susceptibilities in three loess/palaeosol profiles in the Czech Republic; methodological implications. Stud. Geophys. Geod. 62, 272–290. https://doi.org/10.1007/s11200-017-0701-y.

Hu, B., Li, G., Li, J., Bi, J., Zhao, J., Bu, R., 2012. Provenance and climate change inferred from Sr–Nd–Pb isotopes of late Quaternary sediments in the Huanghe (Yellow River) Delta. Quaternary Res. China. https://doi.org/10.1016/j.yqres.2012.07.005.

Jackson, M., Moskowitz, B., Rosenbaum, J., Kissel, C., 1998. Field-dependence of AC susceptibility in titanomagnetites. Earth Planet. Sci. Lett. 157, 129–139.

Jackson, M., 2003–2004.. Imaginary susceptibility, a primer. IRM Q. 13 (1), 10–11.

Jickells, T.D., An, Z.S., Andersen, K.K., Baker, A.R., Bergametti, G., Brooks, N., Cao, J.J., Boyd, P.W., Duce, R.A., Hunter, K.A., Kawahata, H., Kubilay, N., LaRoche, J., Liss, P.S., Mahowald, N., Prospero, J.M., Ridgwell, A.J., Tegen, I., Torres, R., 2005. Global iron connections between desert dust, ocean biogeochemistry, and climate. Sciencem 308, 67–71. https://doi.org/10.1126/science.1105959.

Kapp, P., Pullen, A., Pelletier, J.D., Russell, J., Goodman, P., Cai, F.L., 2015. From dust to dust: quaternary wind erosion of the Mu Us Desert and Loess Plateau China. Geology 43 (9), 835–838. https://doi.org/10.1130/G36724.1.

Kok, J.F., Ridley, D.A., Zhou, Q., Miller, R.L., Zhao, C., Heald, C.L., Ward, D.S., Albani, S., Haustein, K., 2017. Smaller Desert dust cooling effect estimated from analysis of dust size and abundance. Nat. Geosci. 10, 274–281. https://doi.org/10.1038/ngeo2912.

Li, X., Dong, G., Jin, H., Su, Z., Wang, Y., 1999. Discovery of Ordos Cretaceous dune rock and its significance. Chin. Sci. Bull. 44, 2102–2106.

Licht, A., Pullen, A., Kapp, P., Abell, J., Giesler, N., 2016. Eolian cannibalism: Reworked loess and fluvial sediment as the main sources of the Chinese Loess Plateau. Geological Soc. Am. 128, 944–965. https://doi.org/10.1130/B31375.1.

Liu, Y., Yang, S., 2000. Upper TriassiceJurassic sequence stratigraphy and its structural controls in the western Ordos Basin, China. Basin Res. 12, 1–18. https://doi.org/10.1046/j.1365-2117.2000.00107.x.

Liu, Q., Jackson, M.J., Banerjee, S.K., Maher, B.A., Deng, C., Pan, Y., Zhu, R., 2004. Mechanism of the magnetic susceptibility enhancements of the Chinese loess. J. Geophys. Res. 109, B12107. https://doi.org/10.1029/2004JB003249.

Liu, Q., Torrent, J., Maher, B.A., Yu, Y., Deng, C., Zhu, R., Zhao, X., 2005a. Quantifying grain size distribution of pedogenic magnetic particles in Chinese loess and its significance for pedogenesis. J. Geophys. Res. https://doi.org/10.1029/2005JB003726.

Liu, Q., Deng, C., Yu, Y., Torrent, J., Jackson, M.J., Banerjee, S.K., Zhu, R., 2005b. Temperature dependence of magnetic susceptibility in an argon environment: Implications for pedogenesis of Chinese loess/paleosols. Geophys. J. Int. 161, 102–112. https://doi.org/10.1111/j.1365-246X.2005.02564.x.

Liu, Q., Sun, Y., Qiang, X., Tada, R., Hu, P., Duan, Z., Jiang, Z., Liu, J., Su, K., 2015. Characterizing magnetic mineral assemblages of surface sediments from major Asian dust sources and implications for the Chinese loess magnetism. Earth Planets Space 67, 61. https://doi.org/10.1186/s40623-015-0237-8.

Liu, X., Lu, R., Lü, Z., Du, J., Jia, F., Li, T., Chen, L., Wu, Y., 2017. Magnetic susceptibility of surface soils in the Mu Us Desert and its environmental significance. Aeolian Res. 25, 127–134. https://doi.org/10.1016/j.aeolia.2017.04.003.

Lu, H.Y., Wang, X.Y., Li, L.P., 2010. Aeolian sediment evidence that global cooling has driven late Cenozoic stepwise aridification in central Asia. Geological Society, London, Special Publications 342 (1), 29–44.

Loveley, M.R., Marcantonio, F., Wisler, M.M., Hertzberg, J.E., Schmidt, M.W., Lyle, M., 2017. Millennial-scale iron fertilization of the eastern equatorial Pacific over the past 100,000 years. Nat. Geosci. 10, 760–764. https://doi.org/10.1038/NGEO3024.

Maher, B.A., 1988. Magnetic properties of some synthetic sub-micron magnetites. Geophys. J. 94, 83–96. https://doi.org/10.1111/j.1365-246X.1988.tb03429.x.

Maher, B.A., 1998. Magnetic properties of modern soils and Quaternary loessic paleosols: Paleoclimatic implications. Palaeogeogr. Palaeoclimatol. Palaeoecol. 137, 25–54.

Maher, B.A., 2007. Environmental magnetism and climate change. Contemp. Phys. 48 (5), 247–274. https://doi.org/10.1080/00107510801889726.

Maher, B.A., Mitch, T.J., Cunningham, D., 2009. Magnetic and geochemical characteristics of Gobi Desert surface sediments: Implications for provenance of the Chinese Loess Plateau. Geological Soc. Am. 37 (3), 279–282. https://doi.org/10.1130/G25293A.1.

Maher, B.A., 2011. The magnetic properties of Quaternary aeolian dusts and sediments, and their paleoclimatic significance. Aeolian Res. 3, 87–144. https://doi.org/10.1016/j.aeolia.2011.01.005.

Marković, S.B., Stevens, T., Kukla, G.J., Hambach, U., Fitzsimmons, K.E., Gibbard, P., Buggle, B., Zech, M., Guo, Z., Hao, Q., Wu, H., Dhand, K.O., Smalley, I.J., Ujvari, G., Sumegi, P., Timar-Gabor, A., Veres, D., Sirocko, F., Vasiljevic, D.A., Jary, Z., Svensson, A., Jovic, V., Lehmkuhl, F., Kovacs, J., Svircev, Z., 2015. Danube loess stratigraphy – Towards a pan-European loess stratigraphic model. Earth Sci. Rev. 148, 228–258. https://doi.org/10.1016/j.earscirev.2015.06.005.

Nie, J., King, J.W., Fang, X., 2007. Enhancement mechanisms of magnetic susceptibility in the Chinese red-clay sequence. Geophys. Res. Let. 34, L19705. https://doi.org/10.1029/2007GL031430.

Nie, J., King, J., Jackson, M., Fang, X., Song, Y., 2008. AC magnetic susceptibility studies of Chinese red clay sediments between 4.8 and 4.1 Ma: Paleoceanographic and

paleoclimatic implications. J. Geophys. Res. 113, B10106. https://doi.org/10.1029/2008JB005654.
Nie, J., Song, Y., King, J.W., Fang, X., Heil, C., 2010. HIRM variations in the Chinese red-clay sequence: Insights into pedogenesis in the dust source area. J. Asian Earth Sci. 38, 96–104. https://doi.org/10.1016/j.jseaes.2009.11.002.
Nie, J., Horton, B.K., Saylor, J.E., Mora, A., Mange, M., Garzione, C.N., Basu, A., Morena, C.J., Caballero, V., Parra, M., 2012. Integrated provenance analysis of a convergent retroarc foreland system: U-Pb ages, heavy minerals, Nd isotopes, and sandstone compositions of the Middle Magdalena Valley basin, northern Andes, Colombia. Earth Sci. Rev. 110, 111–126. https://doi.org/10.1016/j.earscirev.2011.11.002.
Nie, J., Peng, W., 2014. Automated SEM–EDS heavy mineral analysis reveals no provenance shift between glacial loess and interglacial paleosol on the Chinese Loess Plateau. Aeolian Res. 13, 71–75. https://doi.org/10.1016/j.aeolia.2014.03.005.
Nie, J., Stevens, T., Rittner, M., Stockli, D., Garzanti, E., Limonta, M., Bird, A., Ando, S., Vermeesch, P., Saylor, J., Lu, H., Breecker, D., Hu, X., Liu, S., Resentini, A., Vezzoli, G., Peng, W., Carter, A., Jil, S., Pan, B., 2015. Loess plateau storage of northeastern tibetan plateau-derived yellow river sediment. Nat. Commun. 6, 8511. https://doi.org/10.1038/ncomms9511.
Nie, J., Song, Y., King, J.W., 2016. A review of recent advances in red-clay environmental magnetism and paleoclimate history on the chinese loess plateau. Front. Earth Sci. 4, 1–13. https://doi.org/10.3389/feart.2016.00027.
Nie, J., Pullen, A., Garzione, C.N., Peng, W., Wang, Z., 2018. Pre-Quaternary decoupling between Asian aridification and high dust accumulation rates. Sci. Adv. 4. https://doi.org/10.1126/sciadv.aao6977.
Pokorný, J., Pokorný, P., Suza, P., Hrouda, F., 2011. A multi-function kappabridge for high precision measurement of the AMS and the variations of magnetic susceptibility with field, temperature and frequency. The Earth's Magnetic Interior, IAGA Special Sopron Book Series 1. https://doi.org/10.1007/978-94-007-0323-0_20.
Porter, C.S., 2001. Chinese loess record of monsoon climate during the last glacial-interglacial cycle. Earth Sci. Rev. 54, 115–128. https://doi.org/10.1016/S0012-8252(01)00043-5.
Pullen, A., Kapp, P., McCallister, A.T., Chang, H., Gehrels, G.E., Garizione, C.N., 2011. Qaidam Basin and northern Tibetan Plateau as dust sources for the Chinese Loess Plateau and paleoclimatic implications. Geology 39, 1031e1034. https://doi.org/10.1130/G32296.1.
Qian, P., Zheng, X., Cheng, J., Han, Y., Dong, Y., Zhang, J., 2018. Tracing the provenance of aeolian loess in the Yangtze River Delta through zircon U-Pb age and geochemical investigations. J. Mountain Sci. 15, 708–721. https://doi.org/10.1007/s11629-017-4437-5.
Rao, W., Chen, J., Yang, J., Ji, J., Li, G., Tan, H., 2008. Sr–Nd isotopic characteristics of eolian deposits in the Erdos Desert and Chinese Loess Plateau: Implications for their provenances. Geochem. J. 42, 273–282.
Ravi, S., Gonzales, H.B., Buynevich, I.V., Li, J., Sankey, J.B., Dukes, D., Wang, G., 2019. On the development of a magnetic susceptibility based tracer for aeolian sediment transport research. Earth Surf. Proc. Land. 44, 672–678. https://doi.org/10.1002/esp.4536.
Rea, D.K., Snoeckx, H., Josph, L.H., 1988. Late Cenozoic eolian deposition in the North Pacific: Asian drying, Tibetan uplift, and cooling of the northern hemisphere. Paleoceanography 13, 215–224.
Snowball, I., 1999. Electromagnetic units and their use in environmental magnetic studies. In: F. Oldfield, J. Walden & J. Smith (eds.) Environmental Magnetism: a practical guide. Quaternary Research Association Technical Guide, no. 6, pp. 89-97.
Stevens, T., Palk, C., Carter, A., Lu, H., Clift, P., D., 2010. assessing the provenance of loess and desert sediments in northern China using U-Pb dating and morphology of detrital zircons. Geological Soc. Am. 122, 1331–1344. https://doi.org/10.1130/B30102.1.
Stevens, T., Carter, A., Watson, T.P., Vermeesch, P., Ando, S., Bird, A.F., Lu, H., Garzanti, E., Cottam, M.A., Sevastjanova, I., 2013. Genetic linkage between the Yellow River, the Mu Us Desert and the Chinese Loess Plateau. Quat. Sci. Rev. 78, 355–368. https://doi.org/10.1016/j.quascirev.2012.11.032.
Sun, J., Liu, T., 2000. Multiple origins and interpretations of the magnetic susceptibility signal in Chinese wind-blown sediments. Earth Planetary Sci. Lett. 180, 287–296.
Sun, J., 2002. Provenance of loess material and formation of loess deposits on the Chinese Loess Plateau. Earth Planet. Sci. Lett. 203, 845–859. https://doi.org/10.1016/S0012-821X(02)00921-4.
Sun, Y., Tada, R., Chen, J., Liu, Q., Toyoda, S., Tani, A., Ji, J., Isozaki, Y., 2008. Tracing the provenance of fine-grained dust deposited on the central Chinese Loess Plateau. Geophys. Res. Lett. 35, L01804. https://doi.org/10.1029/2007GL031672.
Sun, Y., Chen, H., Tada, R., Weiss, D., Lin, M., Toyoda, S., Yan, Y., Isozaki, Y., 2013. ESR signal intensity and crystallinity of quartz from Gobi and sandy Deserts in East Asia and implication for tracing Asian dust provenance. Geochem. Geophys. Geosyst. 14, 2615–2627. https://doi.org/10.1002/ggge.20162.
Sun, Y., Yan, Y., Nie, J., Li, G., Shi, Z., Qiang, X., Chang, H., An, Z., 2020. Source-to-sink fluctuations of Asian aeolian deposits since the late Oligocene. Earth Sci. Rev. 200, 102963. https://doi.org/10.1016/j.earscirev.2019.102963.
Vinoj, V., Rasch, P.J., Wang, H., Yoon, J., Ma, P., Landu, K., Singh, B., 2014. Short-term modulation of Indian summer monsson rainfall by West Asian dust. Nat. Geosci. 7, 308–313. https://doi.org/10.1038/NGEO2107.
Wang, G., Li, J., Ravi, S., Van Pelt, R.S., Costa, P.J.M., Dukes, D., 2017a. Tracer techniques in aeolian research: Approaches, applications, and challenges. Earth Sci. Rev. 17, 1–16. https://doi.org/10.1016/j.earscirev.2017.05.001.
Wang, F., Zhao, X., Gerlein-Safdi, C., Mu, Y., Wang, D., Lu., 2017b. Global sources, emissions, transport and deposition of dust and sand and their effects on the climate and environment: A review. Front. Environ. Sci. Eng. 11. https://doi.org/10.1007/s11783-017-0904-z.
Wang, Z., Wu, Y., Tan, L., Fu, T., Wen, Y., Li, D., 2019a. Provenance studies of aeolian sand in Mu Us Desert based on heavy-mineral analysis. Aeolian Res. 40, 15–22.
Wang, Y., Jia, J., Lu, H., Lu, C., Xia, D., 2019b. Fluvial sediments in the Alagxa Plateau as a dust source: Iron mineralogical and geochemical evidence. J. Arid Land 11, 217–227. https://doi.org/10.1007/s40333-019-0125-3.
Zan, J., Fang, X., Li, X., Yan, M., Kang, J., 2019. Long-Term Variations in the Lithogenic Susceptibility of Chinese Eolian Deposits Since the Late Pliocene. Geophys. Res. Lett. 46, 726–735. https://doi.org/10.1029/2018GL080726.
Zhang, H.Z., Lu, H.Y., Yi, S.W., Xu, Z.W., Zhou, Y.L., Tan, H.B., 2013. Zircon typological analyses of the major Deserts/sand fields in Northern China and its implication for identifying sediment source. Quaternary Sci. 33 (2), 334–344.
Zhang, H., Lu, H., Xu, X., Liu, X., Yang, T., Stevens, T., Bird, A., Xu, Z., Zhang, T., Lei, F., Feng, H., 2016. Quantitative estimation of the contribution of dust surces to Chinese loess using detrital zircon U-Pb age patterns. J. Geophys. Res. Earth Surf. 121, 2085–2099. https://doi.org/10.1002/2016JF003936.
Zhang, H. Z., Lu, H. Y., Stevens, T., Feng, H., Fu, Y., Geng, J. Y., & Wang, H. L., 2018. Expansion of dust provenance and aridification of Asia since ~7.2 Ma revealed by detrital zircon U-Pb dating. Geophysical Research Letters, 45(24), 13,437-413,448. https://doi.org/10.1029/2018GL079888.
Zhao, G., Sun, M., Wilde, S.A., Sanzhong, L., 2005. Late Archean to Paleoproterozoic evolution of the North China Craton: Key issues revisited. Precambr. Res. 136 (2), 177–202. https://doi.org/10.1016/j.precamres.2004.10.002.
Zhao, G., Han, Y., Liu, X., Chang, L., Lu, B., Chen, Q., Guo, X., Yan, J., Yan, J., 2016. Can the magnetic susceptibility record of Chinese Red Clay sequence be used for palaeomonsoon reconstructions? Geophus. J. Int. 204, 1421–1429. https://doi.org/10.1093/gji/ggv510.
Özdemir, Ö., Dunlop, D.J., Berquo, T.S., 2008. Morin transition in hematite: Size dependence and thermal hysteresis. Geochem. Geophys. Geosyst. 9, Q10Z01. https://doi.org/10.1029/2008GC002110.